

## Structure-based identification of novel human $\gamma$ -glutamylcysteine synthetase inhibitors

David Hamilton, Jian Hui Wu and Gerald Batist

Departments of Oncology, Pharmacology and Therapeutics, McGill University; Montreal Centre for Experimental Therapeutics in Cancer; Segal Cancer Centre & Lady Davis Institute for Medical Research, Sir Mortimer B. Davis-Jewish General Hospital, Montreal, QC, Canada

Running title: Structural-based identification of novel  $\gamma$ -GCS inhibitors

Corresponding authors: Gerald Batist [Tel: (514) 340-8222, ext. 5418; e-mail gbatist@onc.jgh.mcgill.ca]; [Segal](#) Cancer Centre and Lady Davis Institute for Medical Research, Sir Mortimer B. Davis-Jewish General Hospital, 3755 Cote-Ste-Catherine, Rd., Montreal, QC, Canada, H3T 1E2

Number of text pages: 14

Tables: 1

Figures: 5

References: 26

Word counts: abstract (141), introduction (858), results (1216 )& discussion (232)

Non-standard abbreviations:

MRP-1: multi-drug resistance related protein1; L-BSO: L-buthionine-(R,S)-sulfoximine;  $\gamma$ -GCS<sub>H</sub>:  $\gamma$ -glutamylcysteine synthetase;

## Abstract

Glutathione depletion represents a potentially important strategy to sensitize tumors to cytotoxic drugs. L-buthionine-(R,S)-sulfoximine (L-BSO) has been studied in both pre-clinical and early clinical trials, but limitation on its access has led to a search for alternatives. Using a 3-D molecular model of human the major subunit of the rate-limiting GSH synthetic enzyme  $\gamma$ -glutamylcysteine synthetase ( $\gamma$ -GCS<sub>H</sub>), we virtually screened the NCI chemical database to identify compounds that could bind to and potentially inhibit  $\gamma$ -GCS<sub>H</sub>. We identified 51 test chemicals, all with structures very distinct from BSO. We subjected these compounds to biological assays measuring  $\gamma$ -GCS<sub>H</sub> inhibition and glutathione (GSH) depletion. Among 10 novel  $\gamma$ -GCS inhibitors identified, 4 compounds depleted glutathione in cells, and 2 with related structures sensitized tumor cells to melphalan treatment. This work validates the use of model-based database mining and identified inhibitors of  $\gamma$ -GCS<sub>H</sub> with novel chemical structures.

## Introduction

Glutathione (L- $\gamma$ -glutamyl-L-cysteinyl-glycine) (GSH) is an intracellular tripeptide antioxidant that plays an important role in the maintenance of cellular redox potential and also functions in many other biological processes such as protein and DNA synthesis, detoxification of free radicals, peroxides and endogenous and exogenous toxins, and amino acid transport (Meister and Anderson, 1983; Meister, 1989). The heterodimeric enzyme,  $\gamma$ -glutamylcysteine synthetase ( $\gamma$ -GCS), is composed of heavy ( $\gamma$ -GCS<sub>H</sub>, 637 amino acid) and light ( $\gamma$ -GCS<sub>L</sub>, 274 amino acid) subunits, and catalyzes the first and rate-limiting reaction in GSH biosynthesis.  $\gamma$ -GCS<sub>H</sub> exhibits all the catalytic activity of the native enzyme and is also the site of feedback inhibition by GSH, whereas  $\gamma$ -GCS<sub>L</sub> plays an important regulatory role by increasing substrate affinity. Elevated levels of GSH have been implicated in cellular resistance to alkylating agents, platinum compounds, and irradiation (Griffith and Friedman, 1991). In particular, relative elevations of GSH and  $\gamma$ -GCS have been strongly associated with drug resistance in ovarian tumor cells (Lewandowicz, et al., 2002). Depletion of GSH by L-buthionine-(R,S)-sulfoximine (L-BSO) (**1**, Fig.1), a potent inhibitor of  $\gamma$ -GCS, can reverse drug resistance in these same cells. More recently, GSH and cellular antioxidant capacity have been linked to cellular resistance to topoisomerase inhibitors and to taxanes (Yoshida et al. 2006; Ramanathan et al., 2005). Redox active or generating reagents such as arsenic trioxide have been shown to have enhanced cell killing in the presence of GSH depletion by BSO (Davidson, et al., 2003; Zhu et al., 1999).

Other data suggest that GSH not only functions in a redox capacity in drug resistance, but also conjugates some drugs and renders them substrates for efflux pumps. Rappa *et al* showed that MRP1-overexpressing cells were hypersensitive to L-BSO, which has provided a new rational for the use of  $\gamma$ -GCS inhibitors in the treatment of MRP1-overexpressing tumors (Rappa et al., 2003). This was

subsequently shown again in a kidney epithelial cell line engineered to overexpress MRP1 (Akan et al., 2005).

During phase I clinical trial combining L-BSO and melphalan in heavily pretreated ovarian cancer patients, investigators demonstrated that the treatment was effective at reducing tumour GSH levels, and produced clinical responses in a limited number of previously refractory patients (Dwyer et al., 1996), supporting the view that GSH modulation may represent a novel and effective therapeutic strategy. Preliminary data from a phase II trial of melphalan plus L-BSO in the treatment of metastatic melanoma, performed by Batist et al., demonstrated greater inhibition of  $\gamma$ -GCS and greater depletion of GSH in the tumor compared to the normal peripheral mononuclear cells (Chen et al., 1998).

There have been difficulties in production and availability of BSO, in addition to its limited potency in GSH depletion, and these have stimulated a search for other molecules that can deplete GSH. To date, most studies of BSO analogues have focused on optimizing their potency against *E. coli*  $\gamma$ -GCS (Fig. 1) (Griffith and Mulcahy, 1999; Tokutake et al., 1998). Pentathionine sulfoximine and S-hexyl derivatives (2, Fig.1) display an activity comparable to that of BSO but offer no advantage over BSO (Hiratake, 2002). Compound 3 is a much weaker inhibitor compared with BSO. In particular, compound 4, with R as ethyl, is a very potent inhibitor of *E. coli*  $\gamma$ -GCS, whereas compounds 5 and 6 are more potent than BSO in inhibiting *E. coli* enzyme (Tokutake et al., 1998; Hiratake et al., 2002). Moreover, all of the known  $\gamma$ -GCS inhibitors are effectively based on the BSO skeleton (Fig. 1) and vary in potency and toxicity. In order to continue clinical development of chemosensitizers which inhibit human  $\gamma$ -GCS for GSH depletion, it is desirable to identify novel chemical structures.

Virtual screening is a computational process in which a chemical library containing a large number of (available or virtual) compounds is mined against the three-dimensional (3D) structure of a target of interest to identify potential interactors. Numerous successful applications of virtual screening have been reported (Griffith, 1982; Lynne, 2002). For example, in our previous work (Perola

et al., 2000), a long-forgotten synthetic steroid derivative was identified as a microtubule-stabilizing agent. Since the crystal structure of mammalian  $\gamma$ -GCS<sub>H</sub> has not been solved, it was necessary to build a structural model of human  $\gamma$ -GCS<sub>H</sub>. We recently identified a novel  $\gamma$ -GCS<sub>H</sub> hereditary mutation, R127C, in fibroblasts grown from 2 related patients diagnosed with  $\gamma$ -GCS deficiency, and that led us to generate a model of the putative active site of human  $\gamma$ -GCS<sub>H</sub> (Hamilton et al., 2003). This provided us with the key tool necessary tool for the discovery of new inhibitors using virtual screening.

In this present study, we used our structural model to virtually screen the National Cancer Institute (NCI)-3D chemical database for potential  $\gamma$ -GCS inhibitors. We adopted a multiple-cycle screening strategy that includes both receptor-based and ligand-based methods. Our main objective was to identify novel chemical classes of  $\gamma$ -GCS inhibitors. From 90,000 virtually screened compounds, 51 chemical candidates were physically obtained and subjected to enzymatic and cellular assays. This work led to the identification of 4 novel  $\gamma$ -GCS inhibitors that demonstrated activity in depleting cellular GSH and possess chemical skeletons different from that of BSO. We also showed that GSH depletion resulted in sensitization to a cytotoxic alkylating anti-tumor agent.

## Materials and Methods

### *Virtual Screening*

The 3D structural model of  $\gamma$ -GCS<sub>H</sub> was taken from our previous work (Hamilton et al., 2003). The open part of the NCI-3D database was processed using the Insight II package (Accelrys, Inc., San Diego, CA) with a script (Wu et al., 2001). Specifically, the counter ions were stripped, hydrogen atoms were added and atomic partial charges were assigned using the consistent-valence forcefield. Using the  $\gamma$ -GCS<sub>H</sub> structural model, we virtually screened 90,000 compounds from the processed NCI-3D database, using the software GOLD v2.1 (The Cambridge Crystallographic Data Centre, Cambridge, U.K.), which is a genetic algorithm for calculating the docking modes of small molecules

into protein binding sites (Nissink et al., 2002). The ligand is treated as fully flexible, whereas the proteins were kept rigid except that each Ser, Thr and Tyr hydroxyl group was allowed to rotate to optimize hydrogen-bonding. GoldScore is the default scoring function of GOLD and it was selected to give fitness score for each compound in this work. There are several optimized GOLD parameter settings, which differ in the speed and accuracy for the docking studies: i) the library screen setting is fast with reasonable accuracy; ii) the standard setting is slower than the first one but give more accurate predictions.

The three screening cycles and the overall result of the screenings were summarized by the flow charts in Figure 2. In the first screening cycle, a dataset of 90,000 NCI compounds were reduced to the top 800 compounds by the virtual screen using Gold library screen setting. This dataset of 800 compounds was further reduced to 80 compounds using Gold standard setting. Among the 26 chemical samples subjected to enzymatic assays, 5 initial hits were identified. Next, we screened the NCI-3D database for the analogues of the 5 initial hits, using the ANALOGUE algorithm which was developed locally and is based on a selected set of molecular descriptors. In cycle 2, we identified 5 hits from the 22 analogues of the hits from the first cycle. In cycle 3, we identified 2 lead compounds from the analogues of the hits in cycle 2.

Enrichment curves are obtained by plotting the percentage of inhibitors retrieved as a function of the percentage of total molecules in the dataset. The perfect selection curve (solid line) was plotted by assuming the 11 active compounds in the dataset were ranked as no. 1-11. The random selection curves (white triangles) are defined as the curve that the percentage of the active compounds retrieved is equal to the percentage of the database tested.

### **Chemicals**

L-Buthionine sulfoximine, L-(R,S)-BSO, was purchased from Sigma, and represents the same chiral form used in previous pre-clinical studies. The chemical samples of the NSC compounds were a gift from the Drug Synthesis & Chemistry Branch, DTP, NCI, Bethesda, MD, USA. To verify

MOL #24778

chemical structures of the NSC compounds, we have performed  $^1\text{H}$  NMR and mass spectrum analyses. The  $^1\text{H}$  spectra were recorded on a Bruker AMX2 at 500 MHz. FAB mass spectra were performed with a Quattro II (Micromass Can.) mass spectrometer with a Z-spray interface, at unit resolution, and in the positive ion mode. The samples were dissolved in an acetonitrile/water mixture containing 1% acetic acid. The  $^1\text{H}$  NMR spectra and mass spectrum analyses have confirmed the chemical structures of the active compounds (Table 1). The results are recorded as follows:

Compound NSC21429:  $^1\text{H}$  NMR ( $\text{CDCl}_3$ )  $\delta$  1.42 (t,  $J=7.1$ , 3H), 4.29-4.38 (m, 2H), 7.13 (d,  $J=8.7$  Hz, 1H), 7.18 (d,  $J=8.8$  Hz, 1H), 7.23 (s, 3H), 7.50 (d,  $J=8.7$  Hz, 1H), 7.79 (d,  $J=8.8$ , 1H), 12.07 (s, 1H); MS 241, 242  $[\text{M} + \text{H}]^+$ .

Compound NSC176282:  $^1\text{H}$  NMR ( $\text{CDCl}_3$ )  $\delta$  1.43 (t,  $J=7.1$  Hz, 3H), 4.42 (q,  $J=7.1$  Hz, 2H), 7.37 (d,  $J=8.1$  Hz, 1H), 7.65-7.67 (m, 2H), 13.47 (s, 1H); MS 286, 287  $[\text{M} + \text{H}]^+$ .

Compound NSC266746:  $^1\text{H}$  NMR ( $\text{DMSO}-d_6$ )  $\delta$  4.03 (s, 2H), 7.29-7.32 (m, 1H), 7.36-7.40 (m, 4H), 7.69, (dd,  $J=8.7$ , 2.6 Hz, 1H), 8.08 (s, 1H), 8.19 (br s, 1H), 8.34 (br s, 1H), 8.36 (d,  $J=8.7$  Hz, 1H), 8.41 (d,  $J=2.6$  Hz), 11.62 (s, 1H); MS 314, 315  $[\text{M} + \text{H}]^+$ .

Compound NSC104960:  $^1\text{H}$  NMR ( $\text{DMSO}-d_6$ ) 1.37 (t,  $J=6.7$  Hz, 3H), 4.13 (q,  $J=6.7$  Hz, 2H), 7.37 (dd,  $J=8.3$ , 4.4 Hz, 1H), 7.46 (br s, 1H), 7.52 (d,  $J=8.3$  Hz, 1H), 8.19 (d,  $J=4.4$  Hz, 1H), 8.29 (br s, 1H), 8.45 (s, 1H), 11.61 (s, 1H); MS 224, 225  $[\text{M} + \text{H}]^+$ .

Compound NSC25809:  $^1\text{H}$  NMR ( $\text{DMSO}-d_6$ )  $\delta$  3.93 (s, 3H), 7.34 (s, 1H), 7.73 (s, 2H), 8.01 (s, 1H), 13.0 (s, 1H); MS 228, 229  $[\text{M} + \text{H}]^+$ .

Compound NSC118657:  $^1\text{H}$  NMR ( $\text{CDCl}_3$ )  $\delta$  3.96 (s, 3H), 7.51-7.54 (m, 3H), 7.95 (d,  $J=8$  Hz, 4H), 8.20 (d,  $J=8$  Hz, 2H); MS 240, 241  $[\text{M} + \text{H}]^+$ .

Compound NSC79068:  $^1\text{H}$  NMR ( $\text{CDCl}_3$ )  $\delta$  1.30 (t,  $J=7$  Hz, 3H), 2.75 (q,  $J=7$  Hz, 2H), 7.37 (d,  $J=8$  Hz, 2H), 7.90 (d,  $J=8$  Hz, 2H), 7.96 (d,  $J=8$  Hz, 2H), 8.25 (d,  $J=8$  Hz, 2H); MS 254, 255  $[\text{M} + \text{H}]^+$ .

Compound NSC59492:  $^1\text{H}$  NMR ( $\text{Methanol}-d_4$ )  $\delta$  2.45 (s, 3H), 7.38 (d,  $J=8$  Hz, 2H), 7.86 (d,  $J=8$  Hz, 2H), 7.94 (d,  $J=8$  Hz, 2H), 8.18 (d,  $J=8$  Hz, 2H); MS 240, 241  $[\text{M} + \text{H}]^+$ .



## MOL #24778

Compound NSC24196: MS 236, 237  $[M+H]^+$ ; insoluble in chloroform, low solubility in either DMSO or N,N-Dimethylformamide.

Compound NSC299962:  $^1H$  NMR ( $CDCl_3$ , 500MHz)  $\delta$  6.46 (s, 1H), 4.25 (q, 2H,  $J=7.3$  Hz), 3.65 (s, 2H), 2.32 (s, 1H), 2.16 (s, 3H), 2.08 (s, 3H), 1.32 (t, 3H,  $J=7.3$  Hz); MS 241, 242  $[M+H]^+$ .

### *Cell culture and treatment*

A549 cells were obtained from the American Type Tissue Collection (ATCC) and were cultured in MEM medium (Wisent, St. Bruno, Quebec, Canada) supplemented with non-essential amino acids, 10% fetal bovine serum, sodium pyruvate and penicillin/streptomycin and maintained at 5%  $CO_2$  and 37°C. A549 is an established lung cancer cell line, derived from a human non-small cell lung cancer, has high levels of  $\gamma$ -GCS and GSH and has been shown to express MRP-1 protein in its cell membrane (Torky, et al., 2005).

For each of the drugs, the highest non-toxic dose was determined (L-BSO- 100  $\mu M$ ; NSC59492-90  $\mu M$ ; NSC79068 - 100  $\mu M$ ). For each, the time to maximal GSH depletion was also determined, and in all cases there was no greater depletion beyond 24h, so that the subsequent studies with melphalan were performed using the respective GSH depleter at its highest non-toxic dose, after 24h of exposure. For cytotoxicity determination, cells ( $2 \times 10^3$ ) were seeded into 96-well plates and allowed to attach. The cells were then exposed to medium containing no addition, BSO or the test molecules at the specified doses, for 24 hours. Then the medium was changed, and replaced with fresh medium containing the same addition (nothing, BSO or test molecule), plus serial dilutions of melphalan, and then were left in the incubator for 48 hours, after which the medium was removed and the cells fixed and protein stained using the sulforhodamine blue (SRB) assay. Absorbance was read at 490 nm using an ELX800 microplate reader (Bio-Tek Instruments Inc., Winooski, VT, USA). As control, non-treated, DMSO- and BSO-treated cells were used. We used GraphPad Prism with the exponential decay function to plot best-fit curves for the cell survival data. T-tests were performed to compare each test set to the melphalan alone treated samples.

### ***Recombinant protein production***

The complete cDNA sequence for  $\gamma$ -GCS<sub>H</sub> was kindly provided by Dr. Tim Mulcahy (University of Wisconsin). The  $\gamma$ -GCS<sub>H</sub> cDNA coding sequence was cloned into pet15b (Novagen, USA), and wild-type  $\gamma$ -GCS<sub>H</sub> protein was expressed, purified and quantified as previously described (Hamilton et al., 2003).

### ***Inhibitor activity measurement***

Binding studies utilized a coupled biochemical reaction in which ADP formation is coupled to NADH oxidation as previously described (Hamilton et al., 2003; Wu et al., 2001). For inhibitor K<sub>i</sub> kinetic measurements, compounds were resuspended in DMSO and preincubated with the purified  $\gamma$ -GCS<sub>H</sub> enzyme for 10 minutes at 37°C prior to adding to the reaction buffer. . Reduction in absorbance of NADH at 340nm and 37°C was followed over time using a 96-well plate microplate spectrophotometer (Benchmark Plus, Biorad, Calif., USA). As control, reactions were also performed in complete buffer, without  $\gamma$ -GCS protein. As well, to ensure that the compounds did not directly interact with LDH or PyK, phosphate production was also measured as a means of monitoring activity following the protocol of Kyaw *et al* (Kyaw et al., 1985). Reactions also were performed on native enzyme without compound. Reaction blanks consisted of buffer plus enzyme, but without NADH. Assays were performed in triplicate and data analyzed using a competitive inhibition model analysis. All analyses were performed using Sigma Plot 8.02 software (SPSS Inc.,USA).

For GSH depletion studies, 2 X 10<sup>5</sup> A549 cells were seeded in 60mm dishes and allowed to attach overnight. 24 hours later, fresh media containing test compounds dissolved in DMSO was added. All compounds were used at sub-cytotoxic doses. After incubation for 24-48 hours, cells were washed and harvested and assayed for GSH. As control, non-treated, DMSO- and BSO-treated cells were used.

### ***Glutathione measurement***

Intracellular GSH was measured using the enzymatic-recycling assay (18). Absorbance was read at 405 nm in a 96-well plate format using an ELX800 microplate reader (Bio-Tek Instruments Inc.), and concentrations were determined using purified GSH as standard and expressed as nanomoles of GSH per milligram of protein (nmol/mg protein). Protein concentrations were determined using the BCA (bicinchoninic acid) Protein Assay Kit (Pierce Inc., Rockford, IL, USA).

### ***Comparison of the 3D model of human $\gamma$ GCS with the crystal structure of *E. coli* $\gamma$ GCS***

When this work was initiated, there was no crystal of  $\gamma$ GCS available. Extensive database searches for human  $\gamma$ -GCS<sub>H</sub> using PSI-BLAST<sup>1</sup> did not detect any homologous proteins with known structures. Therefore, we used a fold-recognition method to identify a structure template and built a 3D model of human  $\gamma$ -GCS<sub>H</sub> (Hamilton et al. 2003). The template we identified is the crystal structure of glutamyl-tRNA synthetase (PDB entry: 1gln), which is an oxygen-nitrogen ligase, linking glutamyl to the 3'-OH of the tRNA terminal adenosine.<sup>2</sup> Thus, we used an oxygen-nitrogen ligase as a structural template for a carbon-nitrogen ligase ( $\gamma$ -GCS<sub>H</sub>). This is supported by the observation of Russell et al.<sup>3</sup> that glutaminyl-tRNA synthetase shares a similar fold with one domain of glutamine synthetase, a carbon-nitrogen ligase (Russell and Sternberg, 1997). In the present work, based on the 3D model of human  $\gamma$ -GCS<sub>H</sub>, we identified a series of novel compounds active in inhibiting human  $\gamma$ -GCS, which demonstrates that this 3D model is useful for virtual screening of human  $\gamma$ -GCS inhibitors.

Hibi recently published the crystal structure of *E. coli*  $\gamma$ -GCS. However, there is no significant homology between *E. coli* and human  $\gamma$ -GCS despite catalyzing similar reactions (Hibi et al., 2004). The human  $\gamma$ -GCS is composed of a heavy subunit and a light subunit, where the *E. coli* enzyme is a single 60-kDa polypeptide showing only 8% amino acid sequence identity to the human sequence. Studies of the substrate specificity of *E. coli* and mammalian  $\gamma$ -GCS have indicated that there are differences in the L-Cys binding site, the rate-limiting amino acid in GSH synthesis (Lewandowicz, et

al., 2002). As such, it is not known how well the *E. coli*  $\gamma$ -GCS crystal structure predicts the human homologue, and it has been previously suggested that *E.coli* and *Arabidopsis*  $\gamma$ -GCS proteins may have evolved independently from other species May and Lever, 1994).

On the other hand, L-BSO is a fairly potent inhibitor of both mammalian and *E. coli*  $\gamma$ -GCS (Griffith, 1982; Tokutake, 1998), suggesting that there are similarities in the binding sites of  $\gamma$ -GCS between species. However, by visual inspection we did not identify significant similarity between the 3D model of human  $\gamma$ -GCS and the crystal structure of *E. coli* enzyme. This might be due to either some inaccuracy in the 3D model or structural species differences.

## Results

### *Multiple-cycle Screenings of the National Cancer Institute 3D Database*

The National Cancer Institute (NCI, USA), has a publicly available 3D chemical database that contains more than 200,000 compounds, and consists of unique synthetic chemicals and natural products. Using the  $\gamma$ -GCS<sub>H</sub> structural model we developed on the basis of biological data (Hamilton et al., 2003), we virtually screened 90,000 compounds from the NCI-3D database, using the software Gold (Genetic Optimization for Ligand Docking) and an ANALOGUE algorithm we developed as a functional module of the “Hit Discovery platform. “Hit” compounds were physically obtained from the NCI and tested in biological assays. Any chemical structure that demonstrated GSH-depleting activity was used in subsequent cycles of virtual screening to further identify structural analogues (i.e., ‘guilty by similarity’ strategy), The flow chart for the three screening cycles and the overall results are shown in **Figure 2**. The chemical structures, Ki values, and the percentage of the GSH depletion for the hits of each cycle are reported in Table 1. The time-dependent enzymatic inhibition curves for selected compounds at various doses are shown in Figure 3.

As shown in Fig. 2 and Table 1, the first cycle of screening led to identification of 5 weak hits with the  $K_i$  values in the range of 325.3 to 1420  $\mu\text{M}$ . The  $K_i$  values reported here are the overall inhibition constants. The  $K_i$  value of L-BSO we obtained for the human  $\gamma$ -GCS is 151  $\mu\text{M}$ , whereas the  $K_i$  value of L-BSO for *E. Coli*  $\gamma$ -GCS reported by Tokutake *et al* was 49.3  $\mu\text{M}$ . Even though the hit compounds identified in cycle 1 demonstrated low potency inhibition against  $\gamma$ -GCS, we completed a second round of screening to look for further analogues. We identified a series of potent analogues of NSC176283, NSC185050 and NSC25809 in cycle 2 and cycle 3, and classified these compounds into families A, B and C, respectively (Table 1). Here, several particular points are worthy of note: **a)** NSC21429 is more potent than BSO in enzymatic assays, but it is not active in depleting GSH in cellular assays. This could be due to differences in compound solubility, cell accumulation or metabolism; **b)** NSC104960 has a potency comparable to that of L-BSO in enzymatic assays and more importantly, it is active in depleting GSH levels in A549 cells; **c)** NSC118657, NSC79068 and NSC59492 showed considerable potency in decreasing GSH levels in A549 cells. However, due to the fact that these three compounds are colored, which interfere with our enzymatic assays, we were unable to determine their  $K_i$  values; **d)** Overall, we identified four novel compounds active in depleting GSH in A549 cells, with NSC79068 being the most potent (Table 1); **e)** If we select the  $K_i$  value of NSC185050 (647.1  $\mu\text{M}$ ) as the cutoff for active compounds, and therefore consider NSC176283 and NSC25809 inactive, the total number of the active compounds we identified was 10. In addition, we did not identify active compounds from the analogues of NSC24196 and NSC299962 that we obtained from NCI. But this can not rule out other analogues of NSC24196 and NSC299962.

To investigate time-dependent inhibition profiles of the active compounds, the relative activities were plotted against time for selected compounds at various doses (**Figure 3**). Clearly, inhibition of  $\gamma$ -GCS by L-BSO, NSC21429, NSC104960 and NSC185050 are both time-dependent and dose-dependent. At 500  $\mu\text{M}$  concentration, the time to reach 50% inhibition of the enzyme is

approximately 8, 12, and 5 minutes for L-BSO, NSC21429 and NSC104960, respectively, whereas at 100  $\mu$ M, the time to reach the same extent of inhibition is approximately 27 and 17 minutes for L-BSO and NSC21429, respectively. Therefore, NSC21429 and NSC104960 showed faster binding kinetics than L-BSO at 100  $\mu$ M and 500  $\mu$ M, respectively. In addition, compound NSC185050 is inactive at 100  $\mu$ M but inhibits the enzyme in time-dependent manner at 500  $\mu$ M. This supports the selection of NSC185050 as the cutoff for active compounds.

### ***Compounds NSC59492 and NSC79068 sensitize tumor cells to the treatment of melphalan***

Melphalan is an alkylating chemotherapy agent for which elevated tumor GSH levels can help lead to drug resistance. Compound L-BSO depletes GSH and can reverse melphalan resistance (Lewandowicz et al., 2002). For example, it was shown that L-BSO synergistically reverses melphalan resistance in a group of highly melphalan-resistant neuroblastoma cell lines (Meister and Anderson, 1983). To determine if any of the novel  $\gamma$ -GCS inhibitors we identified could similarly sensitize tumor cells to melphalan treatment, we examined melphalan cytotoxicity in the presence of these compounds, using L-BSO as a positive control. We used each compound's respective highest non-toxic dose, as determined by toxicity studies. Figure 4 shows the results of co-treatment with melphalan in A549 cells. Pretreatment of cells with BSO results in 3.4-fold sensitization. NSC79068 or NSC59492 exposure resulted in smaller (1.5 and 1.4-fold respectively) yet statistically significant decrease in the melphalan IC<sub>50</sub>.

Among the four novel compounds active in depleting cellular GSH (Table 1), NSC79068 and NSC59492 share the same skeleton, and both of them are active in sensitizing tumor cells to the treatment of melphalan.. This suggests that structure family C represented by NSC79068 (Table 1) is a promising chemical class to be optimized as potent inhibitors of human  $\gamma$ -GCS, capable of enhanced chemosensitization. It is note worthy that NSC104960 has a K<sub>i</sub> value of 189.2  $\mu$ M and depleted the GSH level by 21% at 50  $\mu$ M concentration, but it is not active at sensitizing A549 cells to melphalan

toxicity. This could be explained by its weak potency, or the possibility of it being a reversible inhibitor. Consequently, structure class B represented by NSC104960 (Table 1) is another promising chemical class to be investigated further.

### ***Comparison of the 3D model of human $\gamma$ GCS with the crystal structure of *E. coli* $\gamma$ GCS***

To compare the performance of both structures in retrieving known active compounds from a virtual dataset (N=200). First, we compiled a dataset of 200 compounds, which is composed of L-S-BSO, the 10 active compounds we identified (Table 1), 39 inactive compounds which were identified by the enzymatic assays in this work, and 150 compounds which were randomly selected from the NCI database and assumed to be inactive. Next, using either the human 3D model or the crystal structure of *E. coli*  $\gamma$ -GCS, virtual screenings were performed to retrieve the active compounds from the dataset, and the enrichment curves were plotted for two different Gold default screen settings: library screen and standard setting (**Figure 5**).

As shown in Figure 5, the enrichment curves indicate that virtual screening using either the 3D model or the crystal structure of the enzyme are better than random selection at both Gold screen settings. The 3D model of human  $\gamma$ -GCS is better than the crystal structure of *E. coli* enzyme in retrieving the compounds active against human  $\gamma$ -GCS (Figure 5). This might reflect species differences at the enzymatic binding. For the 3D model, the top 10% of the dataset ranked using Gold standard setting (right, Figure 4) was found to retrieve 50% of the active compounds, whereas the top 10% of the dataset using library screen setting (left, Figure 5) was shown to retrieve approximately 42% of the active compounds. Overall, the Gold standard setting is considerably more effective in retrieving the active compounds although it is more computationally expensive than the library screen setting.

## Discussion

Glutathione depletion remains a potentially important strategy for chemosensitization. Recent studies suggest that it may be particularly useful in MRP expressing cells (Rappa et al., 2003; Akan et al., 2005). Most of the pre-clinical studies used BSO as the GSH depleter, and initial clinical trials showed promise (Dwyer et al., 1996; Chen et al., 1998). However, the difficulty in synthesis of BSO has generated interest in identifying other GSH depleters. We are interested in finding entirely new chemical structures which can be used as GSH depleters.

By virtually screening the NCI-3D database using the structural model of human  $\gamma$ -GCS<sub>H</sub> and the strategy to repeatedly search for the analogues of hit compounds, we identified 10 novel compounds active in inhibiting human  $\gamma$ -GCS. Among them, four compounds containing two novel classes of chemical skeletons were shown to deplete GSH levels in A549 tumor cells. Two compounds with related chemical skeletons also resulted in small but significant chemosensitization to melphalan. While this effect is smaller than that of L-BSO, we have nonetheless identified two promising chemical classes, represented by NSC79068 and NSC104960, which can now be further optimized as  $\gamma$ -GCS inhibitors using medicinal chemistry. This will also be the point at which issues of solubility and clinical delivery solvents will be addressed. In addition, we demonstrated that a 3D molecular model can be an effective tool in identifying potential chemical interactors using virtual screening.



## **Acknowledgements**

We are grateful for the chemical samples as a gift from the Drug Synthesis & Chemistry Branch, DTP, NCI, Bethesda, MD. We appreciate the helpful contribution of Andrew Bier.

## References

Akan I, Akan S, Akca H, Savas B, Ozben T. Multidrug resistance-associated protein 1 (MRP1)

mediated vincristine resistance: effects of N-acetylcysteine and Buthionine sulfoximine. *Cancer Cell Int.* 2005 Jul 24;5(1):22.

Chen, X.; Carystinos, G.D. and Batist, G. Potential for selective modulation of glutathione in cancer chemotherapy. *Chemico-Biol. Interactions*, **1998**, 112, 263-275.

Davison K, Mann KK, Waxman S, Miller WH Jr. JNK activation is a mediator of arsenic trioxide-induced apoptosis in acute promyelocytic leukemia cells. *Blood*. **2004**,103(9), 3496-502.

Dwyer, P.J.; Hamilton, T.C.; LaCreta, F.P.; Gallo, J.M.; Kilpatrick, D.; Halbherr, T.; Brennan, J.; Bookman, M.A.; Hoffman, J.; Young, R.C.; Comis, R.L.; Ozols, R.F. Phase I trial of buthionine sulfoximine in combination with melphalan in patients with cancer. *J. Clin. Oncol.*, **1996**, 14, 249-256.

Griffith, O.W. Mechanism of action, metabolism, and toxicity of buthionine sulfoximine and its higher homologs, potent inhibitors of glutathione synthesis. *J. Biol. Chem.*, **1982**, 257, 13704-13712.

Griffith, O.W.; Friedman, H.S. In *Synergism and Antagonism in Chemotherapy*. Chou, T.C., Rideout, D.C., Eds; Academic Press: San Diego, 1991; p 245-285.

Griffth, O.W.; Mulcahy, R.T. The enzymes of glutathione synthesis: gamma-glutamylcysteine synthetase. In *Adv. Enzymol. Relat. Areas Mol. Biol.*, vol. 73; Purich, D.L., Eds; John Wiley & Sons, Inc.: New York, 1999; pp 209-267.

MOL #24778

Hamilton, D.; Wu, J.H.; Alaoui-Jamali, M.; Batist, G. A novel missense mutation in the  $\gamma$ -glutamylcysteine synthetase catalytic subunit gene causes both decreased enzymatic activity and glutathione production. *Blood*, **2003**, 102, 725-730.

Hibi T, Nii H, Nakatsu T, Kimura A, Kato H, Hiratake J, Oda J. Crystal structure of gamma-glutamylcysteine synthetase: insights into the mechanism of catalysis by a key enzyme for glutathione homeostasis. *Proc Natl Acad Sci U S A*. 2004 Oct 19;101(42):15052-7. Epub 2004 Oct 11.

Hiratake, J.; Irie, T.; Tokutake, N.; Oda, J.I. Recognition of a cysteine substrate by E. coli  $\gamma$ -glutamylcysteine synthetase probed by sulfoximine-based transition-state analogue inhibitors. *Biosci. Biotechnol. Biochem.*, **2002**, 66, 1500-1514.

Kyaw, A., Maung-U, K., Toe, T. Determination of inorganic phosphate with molybdate and Triton X-100 without reduction. *Anal. Biochem.*, **1985**, 145, 230-234.

Lewandowicz, G.M.; Britt, P.; Elgie, A.W.; Williamson, C.J.; Coley, H.M.; Hall, A.G.; Sargent, J.M. Cellular glutathione content, in vitro chemoresponse, and the effect of BSO modulation in samples derived from patients with advanced ovarian cancer. *Gynecol. Oncol.*, **2002**, 85 298-304.

Lyne, P.D. Structure-based virtual screening: an overview. *Drug Discovery Today*, **2002**, 7, 1047-1055.

May, M.J. & Leaver, C.J. Arabidopsis thaliana gamma-glutamylcysteine synthetase is structurally unrelated to mammalian, yeast, and Escherichia coli homologs. *Proc Natl Acad Sci U S A*, **1994**, 91, 10059-63.

Meister, A. Metabolism and Function of Glutathione. In *Glutathione: Chemical, Biochemical and Medical Aspects*; Dolphin, D., Avramovich, A., Poulson, R., Eds.; John Wiley & Sons, Inc.: New York, 1989; pp 367-474.

Meister, A.; Anderson, M.E. Glutathione metabolism and function. *Annu. Rev. Biochem.* **1983**, 52, 711-760.

Perola, E.; Xu, K.; Kollmeyer, T.M.; Kaufmann, S.H.; Prendergast, F.G.; Pang, Y.P. Successful virtual screening of a chemical database for Farnesyltransferase inhibitor leads. *J. Med. Chem.*, **2000**, 43, 401.

Ramanathan B, Jan KY, Chen CH, Hour TC, Yu HJ, Pu YS. Resistance to paclitaxel is proportional to cellular total antioxidant capacity. *Cancer Res.* 2005 Sep 15;65(18):8455-60.

Rappa, G.; Gamcsik, M.P.; Mitina, R.L.; Baum, C.; Fodstad, O.; Lorico, A. *Euro. J. Cancer*, **2003**, 39, 120-128.

Skehan P, Storeng R, Scudiero D. *et al.* New colorimetric cytotoxicity assay for anticancer-drug screening. *J Natl Cancer Inst.* **1990**, 82, 1107-12.

Tokutake, N.; Hiratake, J.; Katoh, M.; Irie, T.; Kato, H.; Oda, J.I. Design, synthesis and evaluation of transition-state analogue inhibitors of *Escherichia coli*  $\gamma$ -glutamylcysteine synthetase. *Bioorg. & Med. Chem.*, **1998**, 6, 1935-1953.

Torky, A.R.; Stehfest, E.; Viehweger, K.; Taege, C.; Foth, H. Immuno-histochemical detection of MRPs in human lung cells in culture. *Toxicology* **2005**, 207(3), 437-50.

Wu, J.H.; Batist, G.; Zamir, L.O. Identification of a novel steroid derivative, NSC12983, as a Paclitaxel-like tubulin assembly promoter by 3-D virtual screening. *Anti-Cancer Drug Des.*, **2001**, 16, 129-133.

Wu, J.H.; Batist, G. and Zamir, L.O. Identificaiton of a novel steroid derivative, NSC12983, as a paclitaxel-like tubulin assembly promoter by 3-D virtual screening. *Anti-Cancer Drug Des.*, **2001**, 16, 129-133.

Yoshida A, Takemura H, Inoue H, Miyashita T, Ueda T. Inhibition of glutathione synthesis overcomes Bcl-2-mediated topoisomerase inhibitor resistance and induces nonapoptotic cell death via mitochondrial-independent pathway. *Cancer Res.* 2006 Jun 1;66(11):5772-80.

Zhu XH, Shen YL, Jing YK, Cai X, Jia PM, Huang Y, Tang W, Shi GY, Sun YP, Dai J, Wang ZY, Chen SJ, Zhang TD, Waxman S, Chen Z, Chen GQ. Apoptosis and growth inhibition in malignant lymphocytes after treatment with arsenic trioxide at clinically achievable concentrations. *J Natl Cancer Inst.* 1999 May 5;91(9):743-5.

## Footnotes

This work was supported by Canadian Institute of Health Research via operating grants to G.B. and J.H.W., and by the Réseau de recherche sur le cancer, Fonds de la recherche en santé du Québec.

## Legends for figures

**Figure 1.** Chemical structures of BSO and some of its analogues

**Figure 2. Left) the three screening cycles; Right) the overall result of the screenings.** Cycle 1 is receptor-based, using the  $\gamma$ -GCS<sub>H</sub> molecular model as “bait” in virtual screening, whereas cycles 2 and 3 are ligand-based, testing compounds in vitro for  $\gamma$ -GCS<sub>H</sub> inhibition or cellular GSH depletion.. Notes for each cycle of the screenings: 1) Using software Gold, library screen setting; 2) Gold, standard setting; 3) Visual inspections to reduce the 80 compounds to 49 candidates after excluding compounds containing less than 2 polar atoms (N, O, S); Out of the 49 compounds, 26 chemical samples were obtained from the NCI, Bethesda, MD; 4) Enzymatic assays using recombinant human  $\gamma$ -GCS; 5) Analogues of the initial hits in cycle 1 using ANALOGUE algorithm; 6) Enzymatic assays and cell-based GSH deletion assays; 7) Analogues of the hits in cycle 2; 8) Assays to determine if the compound could sensitize drug-resistant tumor cells to the treatment of melphalan, which were performed for all of the hits from each cycles.

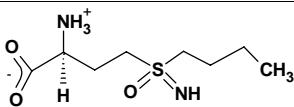
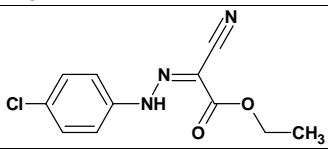
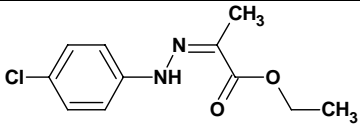
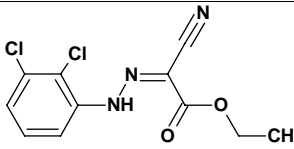
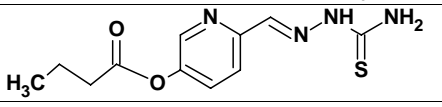
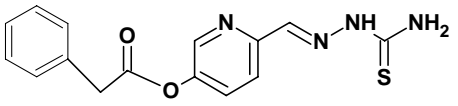
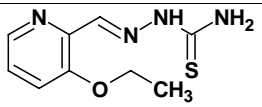
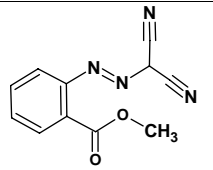
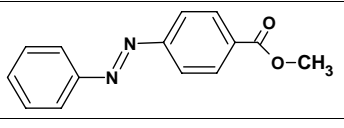
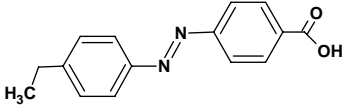
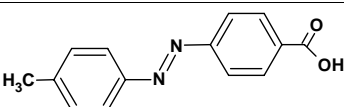
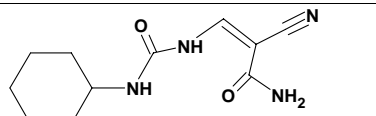
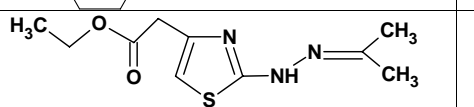
**Figure 3. Time-dependent inhibition curves** for the selected active compounds at various concentrations. Relative activity, is the enzyme activity over time of recombinant and purified  $\gamma$ -GCS<sub>H</sub>.

**Figure 4. Cell survival curves and calculated IC<sub>50</sub> for A549 cells exposed to varying doses of Melphalan +/- BSO, NSC59492, or NSC79068** at their respective highest non-toxic dose. Student's t-test was used to compare each GSH depletor treated test set to the Melphalan alone treated cells.

**Figure 5. Comparison of virtual screening performance by enrichment curves.** The curves represent the percentage of inhibitors retrieved as a function of the percentage of total molecules in the dataset (N=200) for the 3D model of human  $\gamma$ -GCS (white circles) and IVA6, which is the crystal structure of *E coli*  $\gamma$ -GCS (dash lines). The curves were constructed using two different virtual screening settings: Gold: **left)** Gold library screen setting; **right)** Gold standard setting. The curves for perfection selection (solid lines) and random selection (white triangles) are shown.

**Table 1. Chemical structures, Ki and the percentages of GSH decrease of the hits in cycles 1-3.**

(a) The fold was calculated by LD<sub>50</sub> (Melfalphan alone)/LD<sub>50</sub>(Compound with melfalphan) (b)p=0.0003, (c) p=0.057, (d) p=0.006

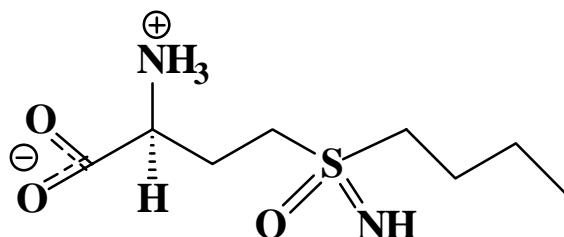
					50 $\mu$ M	100 $\mu$ M
L-BSO				151.3 $\pm$ 43	90	90
Family A	Cycle 1	176283		1420 $\pm$ 153	-	-
	Cycle 2	21429		66.7 $\pm$ 27	-	-
		176282		380.9 $\pm$ 104	-	-
Family B	Cycle 1	185050		647.1 $\pm$ 44	-	-
	Cycle 2	266746		149.1 $\pm$ 51	-	-
		104960		189.2 $\pm$ 38	21	32
Family C	Cycle 1	25809		1350 $\pm$ 61	-	-
	Cycle 2	118657		N.D. <sup>b</sup>	35	56
	Cycle 3	79068		N.D.	71	74
		59492		N.D.	49	54
Other	Cycle 1	24196		414.0 $\pm$ 52	-	-
		299962		325.3 $\pm$ 94	-	-



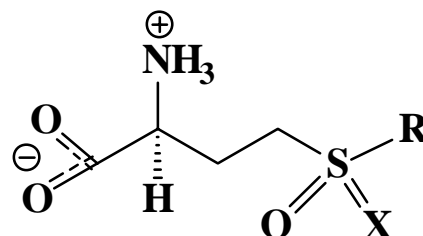
“Binding studies utilized a coupled biochemical reaction, as previously described (ref. 30), in which ADP formation is coupled to NADH oxidation. <sup>b</sup>N.D. = ‘not determined’. <sup>c</sup>Percentage of the decrease in GSH levels after incubation of A549 cells with compounds at 50 and 100  $\mu$ M concentrations, respectively; ‘-’ = inactive.

---

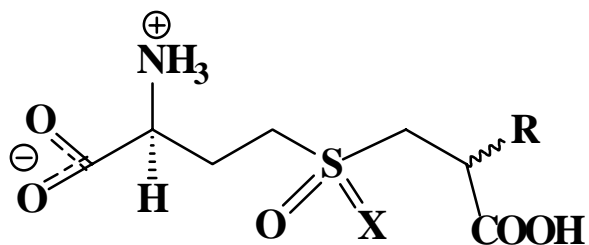
Figure 1



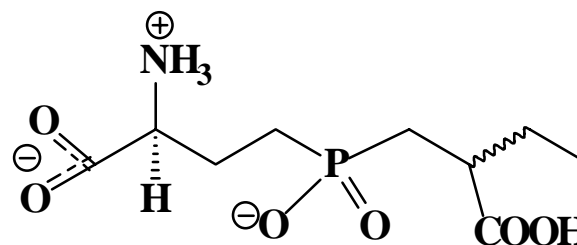
1. L-(R,S)-BSO



2. X=NH; R=(CH<sub>2</sub>)<sub>4</sub>CH<sub>3</sub> Pentathionine sulfoximine  
 X=NH; R=(CH<sub>2</sub>)<sub>5</sub>CH<sub>3</sub> S-hexyl BSO derivative  
 3. X=O; R=(CH<sub>2</sub>)<sub>3</sub>CH<sub>3</sub> L-buthionine sulfone



4. X=NH; R=Me, Et, n-Pr, n-Bu, n-Hex  
 Sulfoximine derivatives  
 5. X=O; R=Et Sulfone



6. Phosphinate

Figure 2

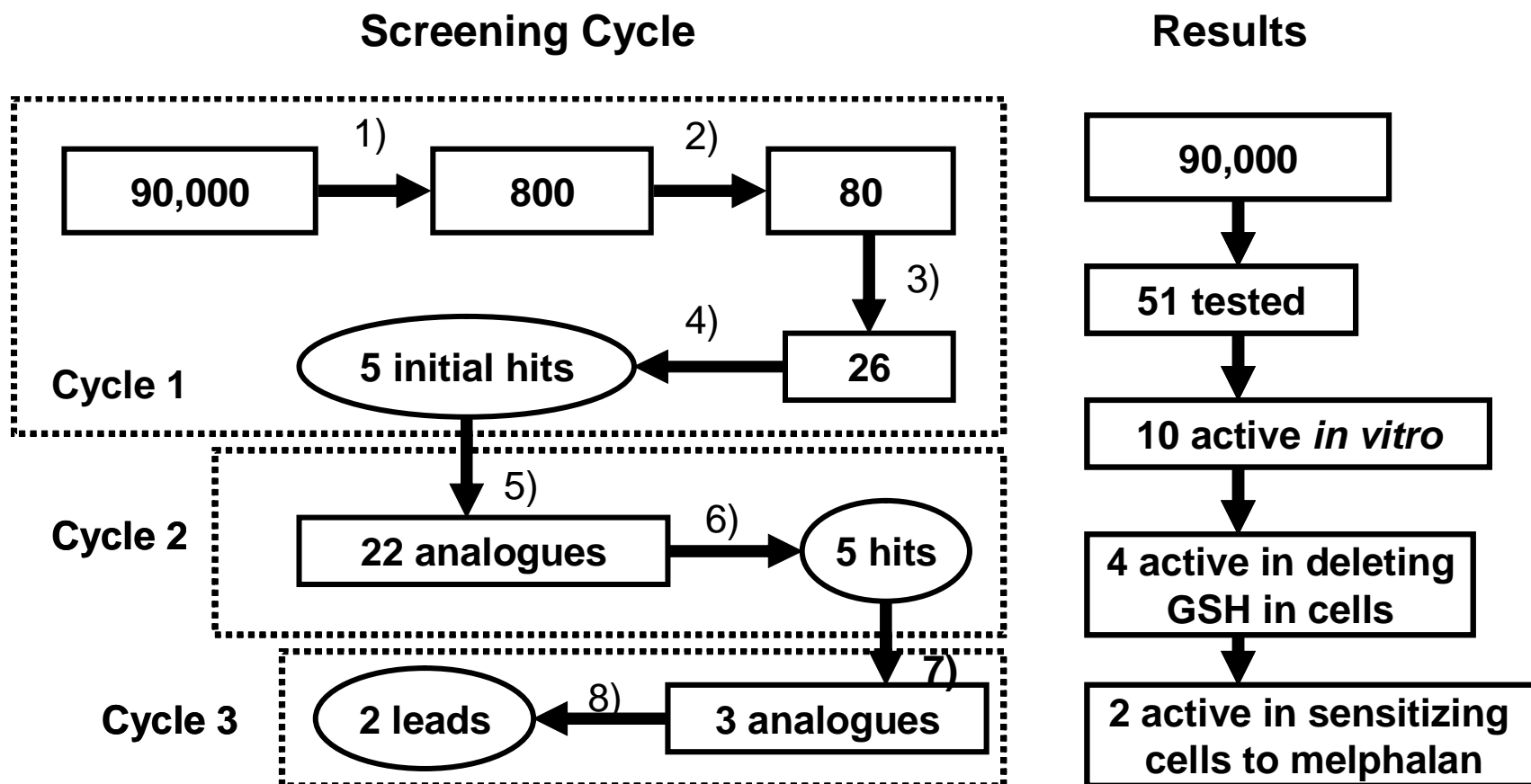
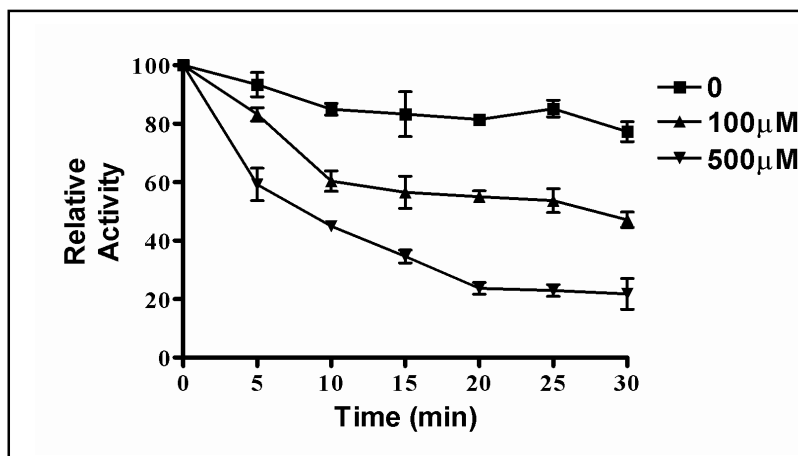
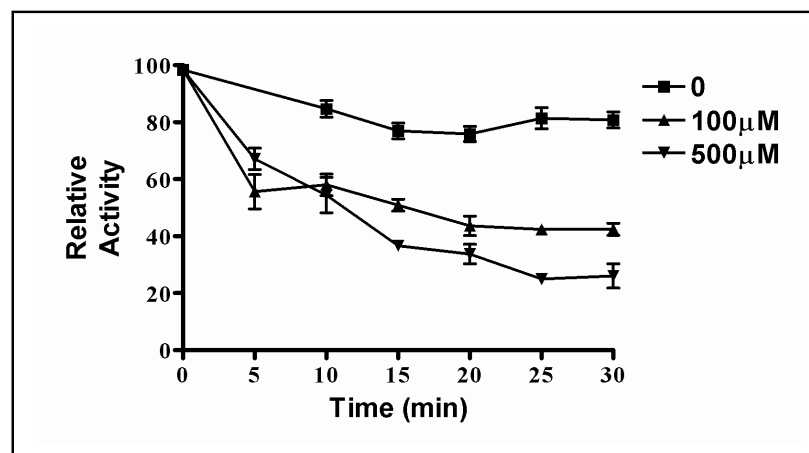


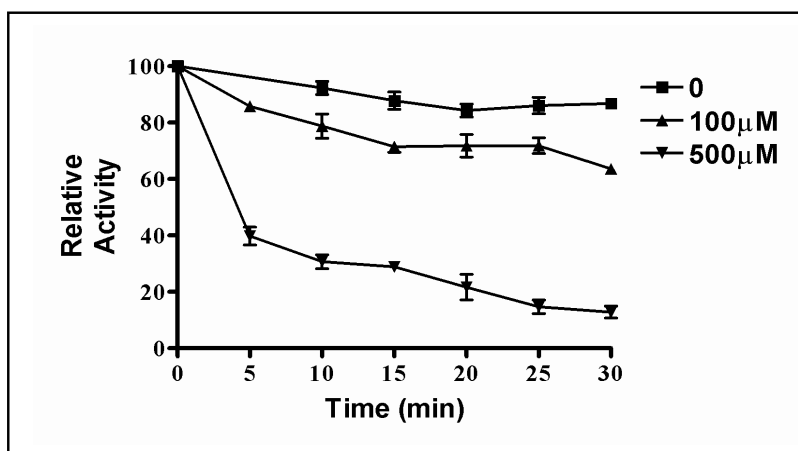
Figure 3



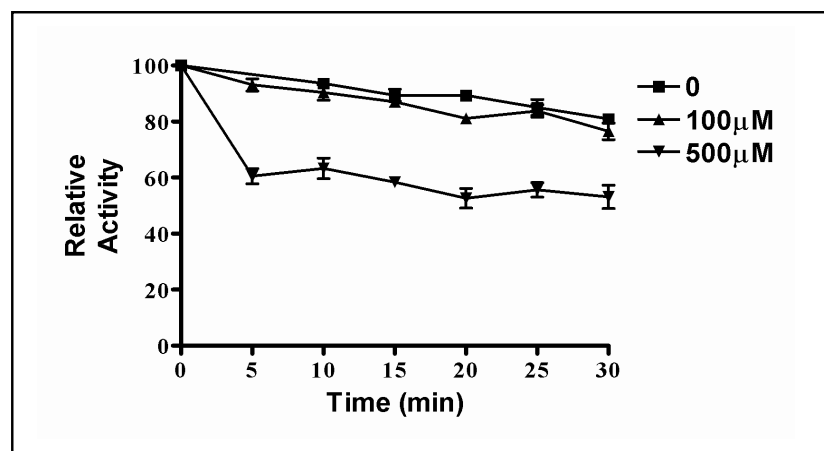
a) L-BSO



b) NSC21429

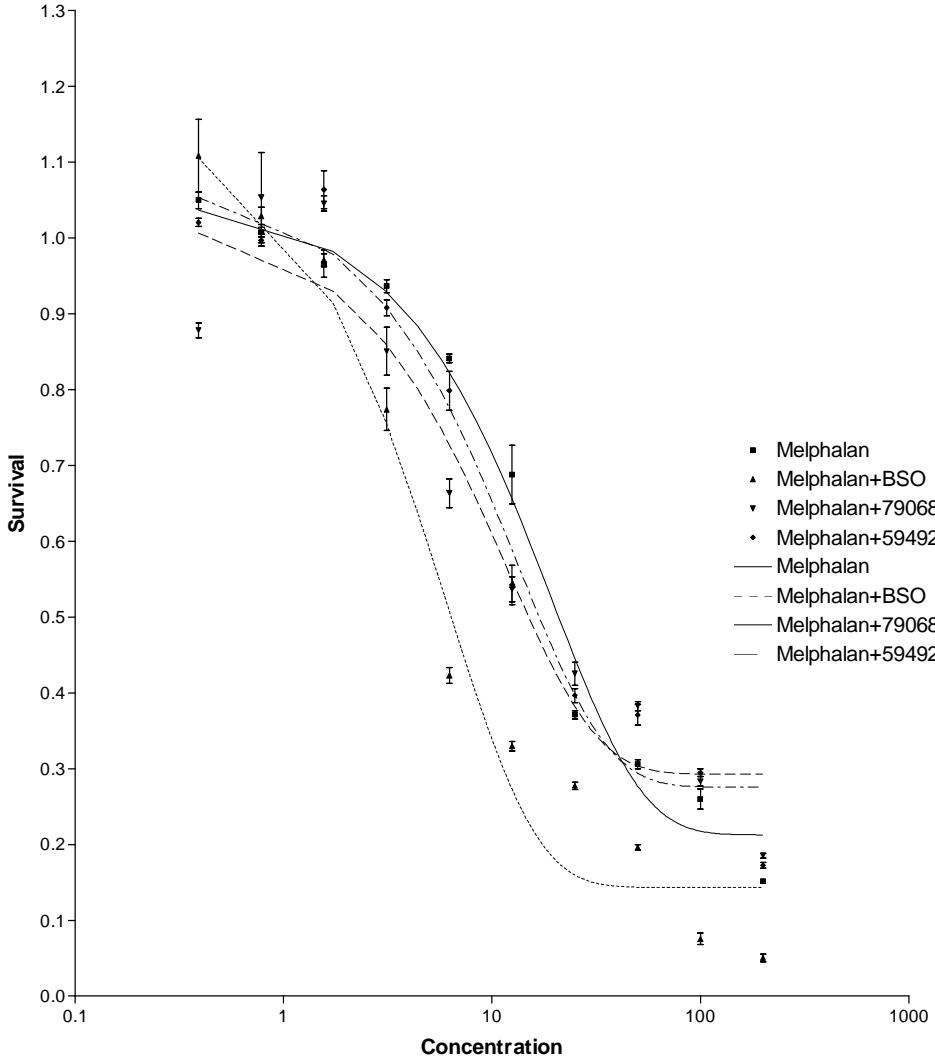


c) NSC104960



d) NSC185050

Figure 4



	Melphalan	Melphalan+BSO	Melphalan+79068	Melphalan+59492
IC <sub>50</sub>	13.50	4.181	8.204	9.203
95% Confidence Intervals	16.04 to 11.65	5.255 to 3.472	11.82 to 6.281	11.45 to 7.694
P value		P<0.001	P<0.001	P<0.001

Figure 5

